Electronic Supplementary Material (ESI) for Energy & Environmental Science.

Supporting Information

Titanium-oxo clusters reinforced gel polymer electrolyte enabling lithium-sulfur batteries with high gravimetric energy densities

Fei Pei,[a] Shuqi Dai,[a] Baofu Guo,[a] Hao Xie,[a] Chaowei Zhao,[a] Jingqin Cui,[a] Xiaoliang Fang,*[a,b] Chengmeng Chen[c,d] and Nanfeng Zheng*[a,b]

[a] Pen-Tung Sah Institute of Micro-Nano Science and Technology, State Key Laboratory for Physical Chemistry of Solid Surfaces, Collaborative Innovation Center of Chemistry for Energy Materials, National & Local Joint Engineering Research Center for Preparation Technology of Nanomaterials, and College of Chemistry and Chemical Engineering, Xiamen University, Xiamen, Fujian 361005, China.
Email: x.l.fang@xmu.edu.cn; nfzheng@xmu.edu.cn

[b] Fujian Science & Technology Innovation Laboratory for Energy Materials of China, Xiamen, Fujian 361005, China.

[c] CAS Key Laboratory of Carbon Materials, Institute of Coal Chemistry, Chinese Academy of Sciences, Taiyuan 030001, China.

[d] University of Chinese Academy of Sciences, Beijing 100049, China.

Experimental

^{7}Li NMR spectroscopy was evaluated with a Bruker Avance III 500 MHz spectrometer. For preparation of the NMR samples, LiTFSI and additives were dissolved in deuterated chloroform ($CDCl_3$) with a concentration of 10 wt%. The resulting solutions were placed into 5 mm borosilicate NMR tubes under a nitrogen atmosphere. Electrochemical stability window was obtained by the linear sweep voltammogram with a two-electrode cell.[S1] In the two-electrode cell, stainless steel was used as the working electrode and Li foil as both the counter electrode and reference electrode, respectively. The activation energy (E_a) of the PVFH-TOC-PEG electrolyte was evaluated by Vogel-Tamman-Fulcher empirical equation.[S2] Ionic conductivity was measured with a Li-ion blocking symmetric cell assembled by sandwiching GPE between two stainless steel electrodes (SS|GPE|SS).[S1] Based on the EIS analysis at a frequency range from 0.1 to 10^6 Hz, the ionic conductivity (σ) is calculated by the following equation:

$$\sigma = \frac{d}{R \times S}$$

Where σ is the ionic conductivity (S cm^{-1}), d is the thickness of the electrolyte, R is the bulk resistance, and S represents the area in contact with the electrodes, respectively. The thickness of GPE used in the ionic conductivity testing is 100 μm.

Li-ion transference number (t_{Li^+}) was measured with a potentiostatic polarization method.[S1] t_{Li^+} is calculated by the following equation:

$$t_{Li}^{+} = \frac{I_{SS}(\Delta V - I_0 R_0)}{I_0(\Delta V - I_{SS} R_{SS})}$$

Where ΔV is the applied polarization voltage (ΔV = 10 mV), I_0 and R_0 are the initial current and interfacial resistance before polarization, respectively, and I_{ss} and R_{ss} are the final state current and interfacial resistance after polarization for 1600 s, respectively.

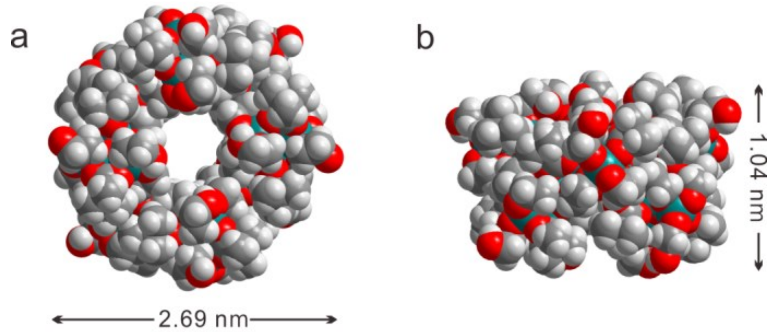

Fig. S1 Crystal structure of the TOC in space-filling model. Color legend: Light gray, H; gray, C; red, O; cyan, Ti.

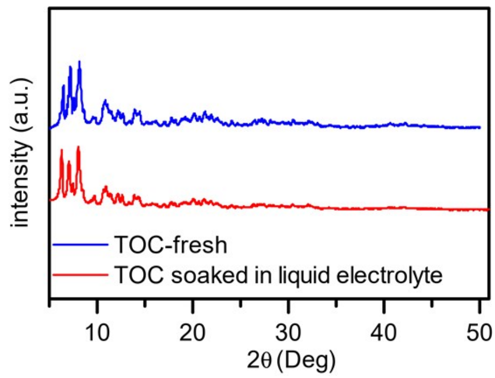

Fig. S2 XRD patterns of the freshly synthesized TOC and the Li-S electrolyte treated TOC.

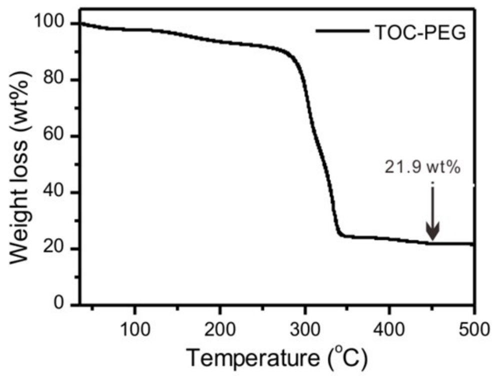

Fig. S3 TG curve of TOC-PEG. According to the average molecular weight of PEG-400 (360~440 g mol^{-1}), the residual amounts of TiO_2 in TOC and TOC-PEG after thermal decomposition are 40.6 wt% and 20.7~23.1 wt%, respectively. Therefore, the TGA result indicated that the vast majority of the EGH ligands in TOC clusters have been exchanged with PEG after the ligand-exchange process.

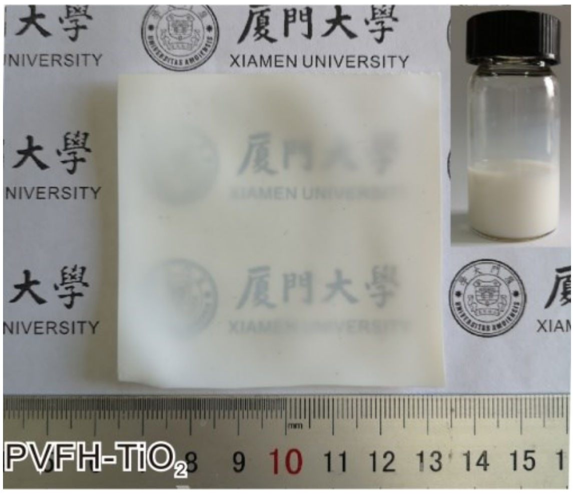

Fig. S4 Optical images of the mixture of PVFH and P25 TiO_2 and the PVFH-TiO_2 membrane with a P25 TiO_2/PVFH ratio of 5/95 (w/w).

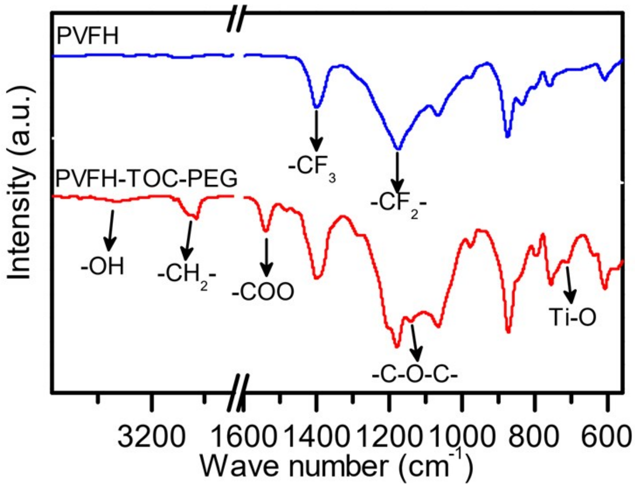

Fig. S5 FTIR spectra of PVFH and PVFH-TOC-PEG.

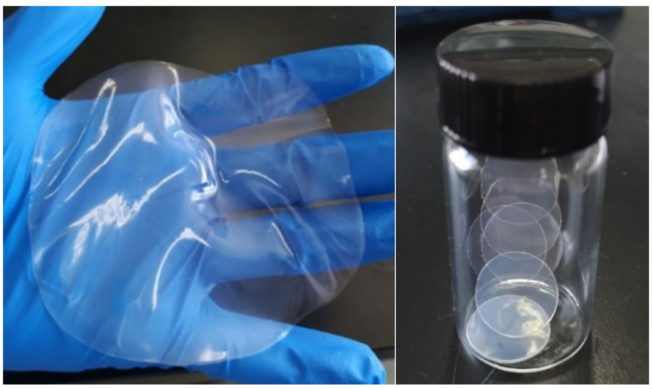

Fig. S6 Optical images of the PVFH-TOC-PEG electrolyte.

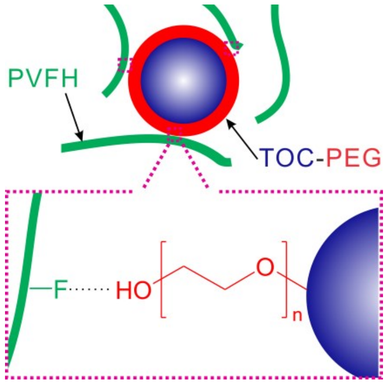

Fig. S7 Schematic illustration of the hydrogen bond between PVFH and TOC-PEG.

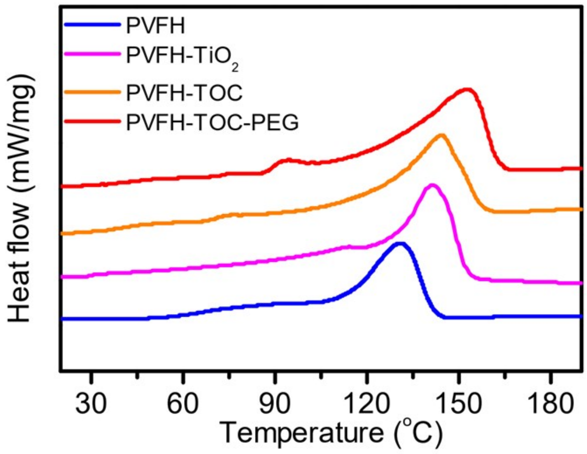

Fig. S8 DSC curves of the PVFH, PVFH-TiO_2, PVFH-TOC and PVFH-TOC-PEG membranes.

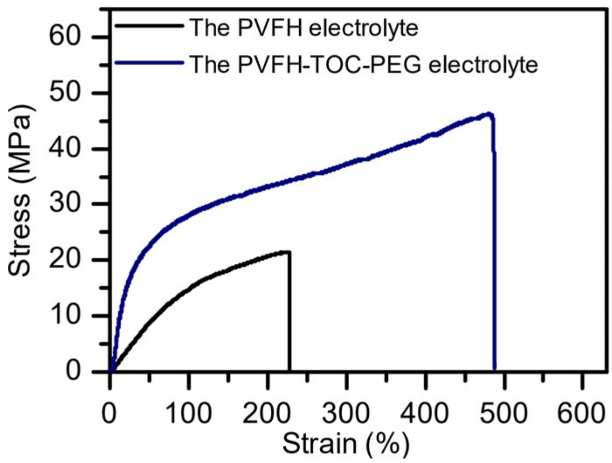

Fig. S9 Stress-strain measurement of the PVFH and PVFH-TOC-PEG electrolytes.

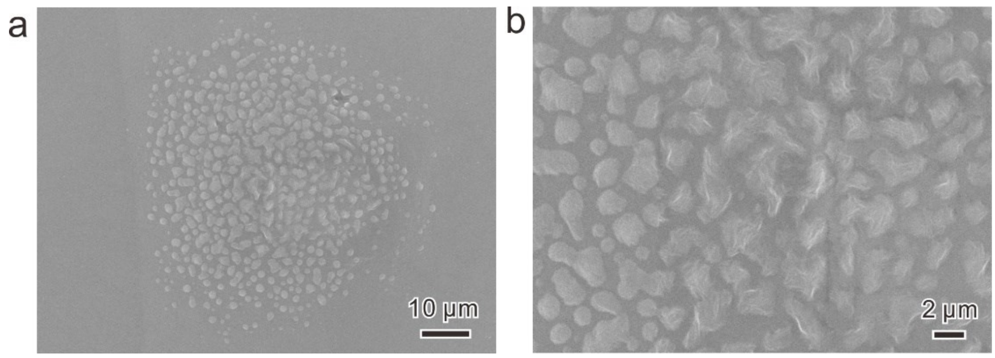

Fig. S10 SEM images of the PVFH-TOC-PEG-10 membrane with a TOC-PEG content of 10 wt%.

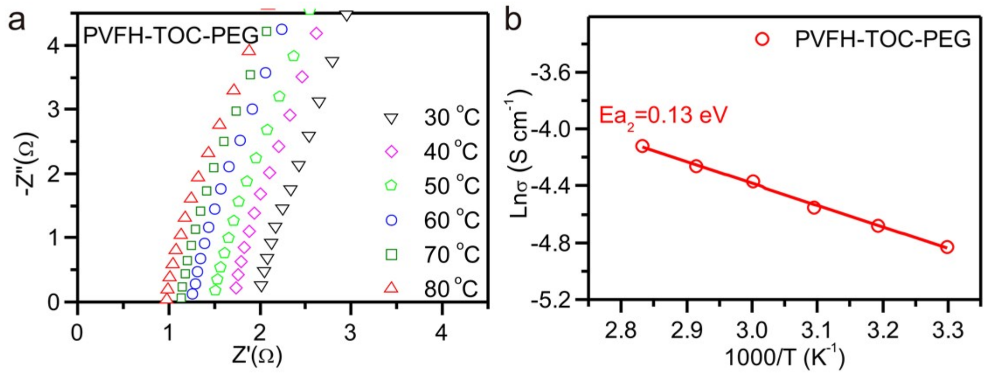

Fig. S11 Temperature-dependent ionic conductivity of the PVFH-TOC-PEG electrolyte.

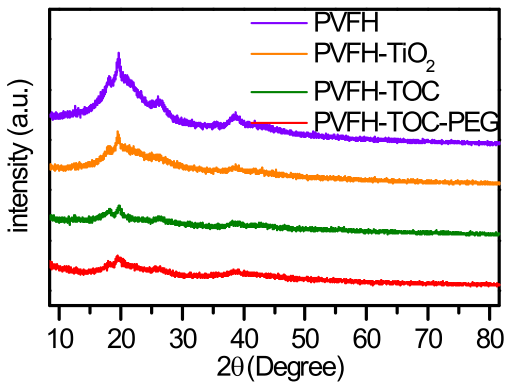

Fig. S12 XRD patterns of the PVFH, PVFH-TiO_2, PVFH-TOC, and PVFH-TOC-PEG membranes.

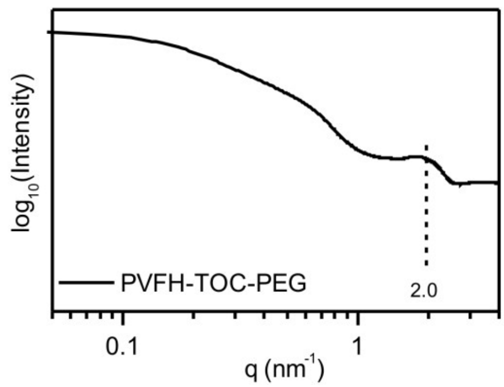

Fig. S13 Small-angle X-ray scattering (SAXS) profile of the PVFH-TOC-PEG membrane. The peak around q = 2.0 nm^{-1} indicates that the scattering originates from particles with an average diameter (d) of 3.14 nm (d = $2\pi/q$).[S2] Considering that the diameter of TOC is 2.69 nm, the SAXS test reveals that TOC-PEG is highly dispersed in the PVFH-TOC-PEG membrane.

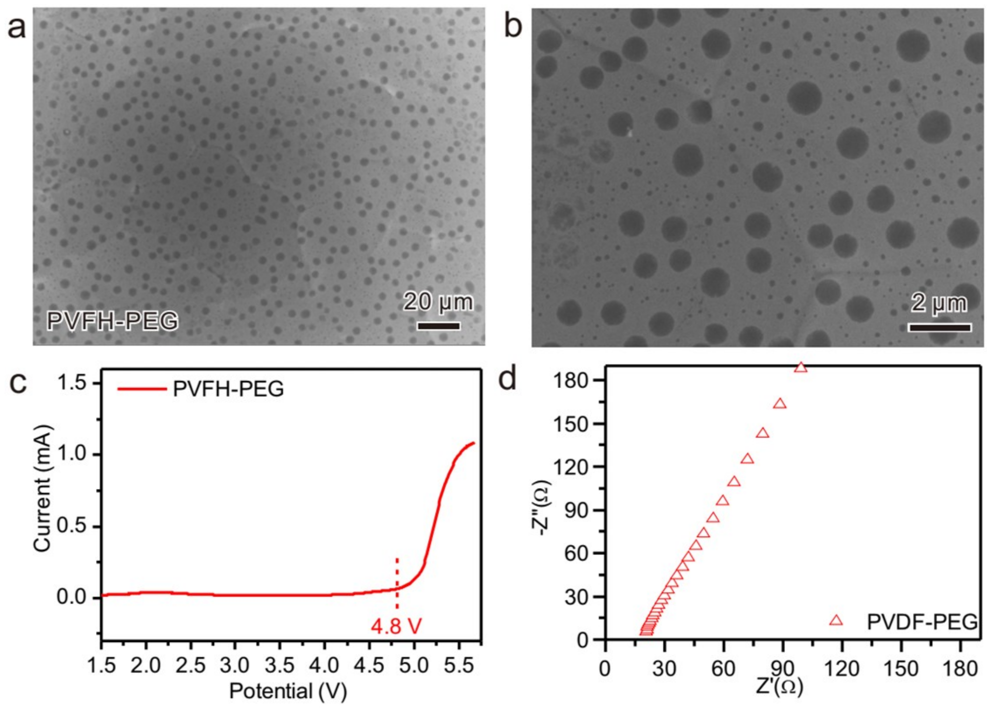

Fig. S14 (a, b) SEM images of the PVFH-PEG membrane. (c) ESW of the PVFH-PEG electrolyte. (d) EIS measurement of the PVFH-PEG electrolyte at 25 °C. The PVFH-PEG membrane was fabricated by mixing PVFH and PEG-400 with a weight ratio of 95/5. Both the ESW (4.8 V) and ionic conductivity (4.8 x 10^{-4} S cm^{-1}) of the PVFH-PEG electrolyte are lower than those of the PVFH-TOC-PEG electrolyte.

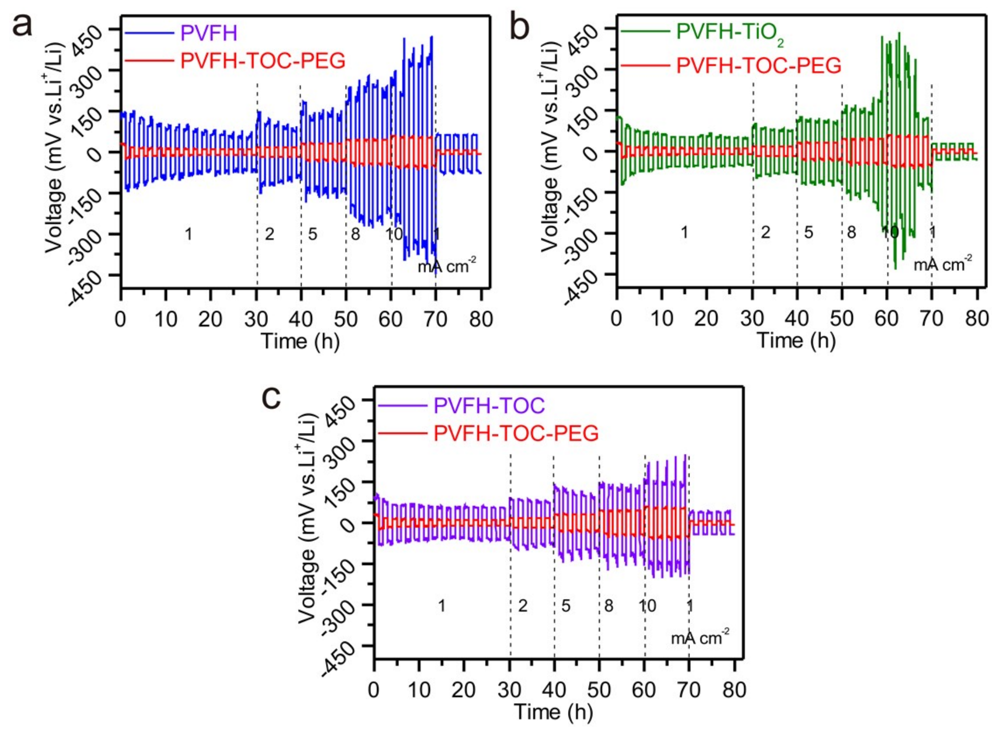

Fig. S15 Rate capabilities of the (a) Li|PVFH|Li, (b) Li|PVFH-TiO_2|Li, and (c) Li|PVFH-TOC|Li cells measured at current densities of 1, 2, 5, 8 and 10 mA cm^{-2}.

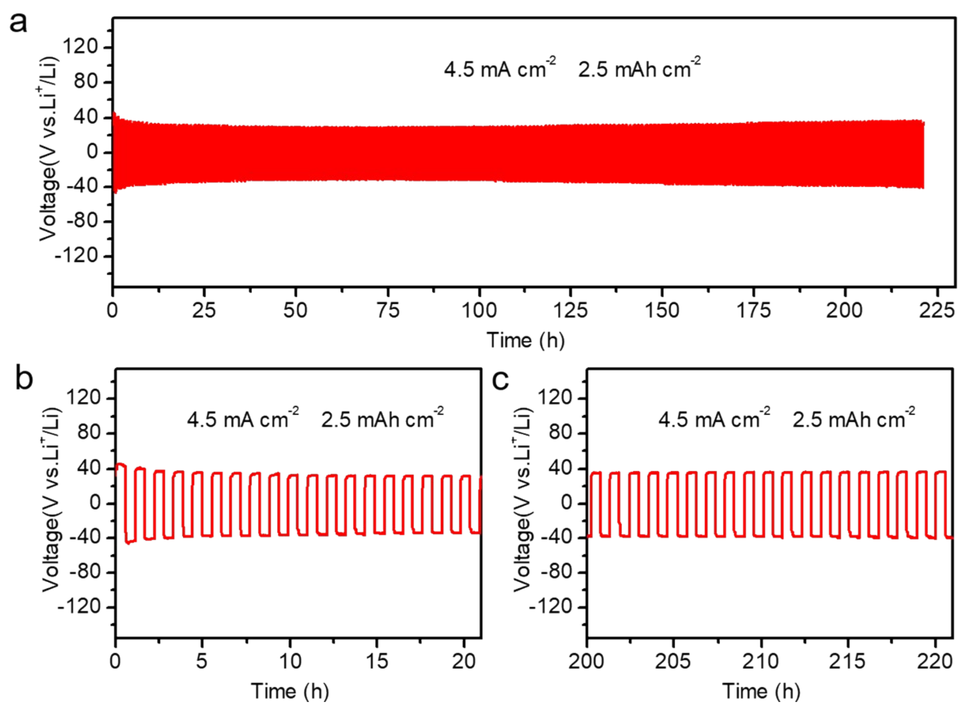

Fig. S16 The cycling stability of the Li|PVFH-TOC-PEG|Li cell at 4.5 mA cm^{-2} and 2.5 mAh cm^{-2}.

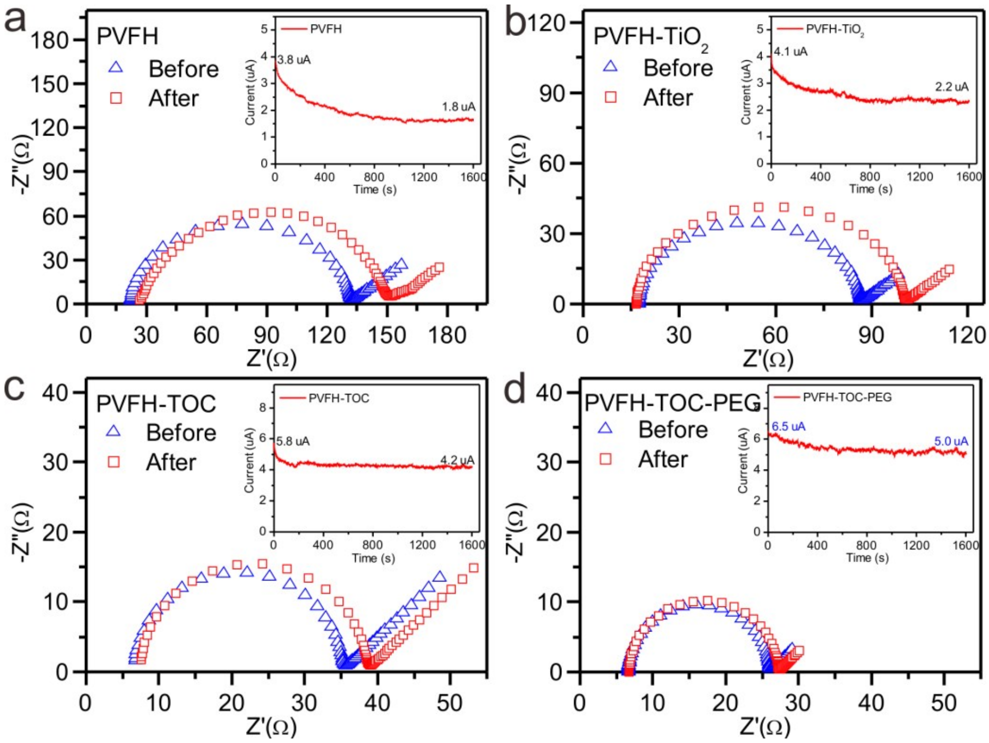

Fig. S17 Measurements of the Li^+ transference numbers of (a) PVFH, (b) PVFH-TiO_2, (c) PVFH-TOC, and (d) PVFH-TOC-PEG.

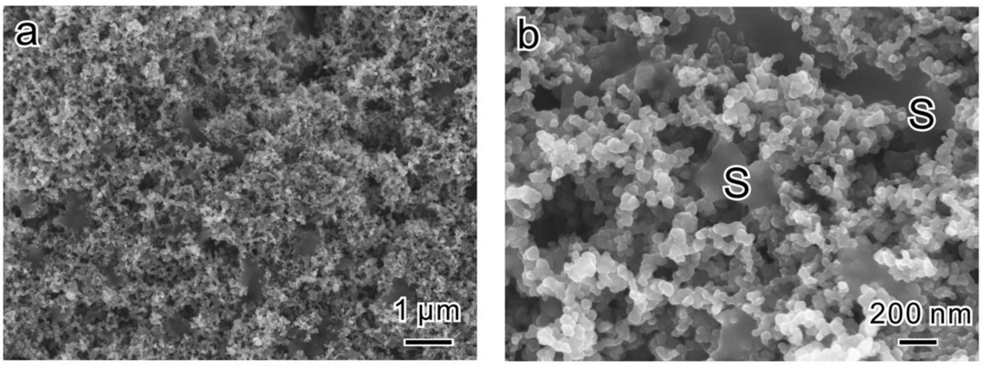

Fig. S18 SEM images of the CB/S composite. Since the sulfur content of the CB/S composite is as high as 84 wt%, some solid sulfur particles can be observed in the SEM images.

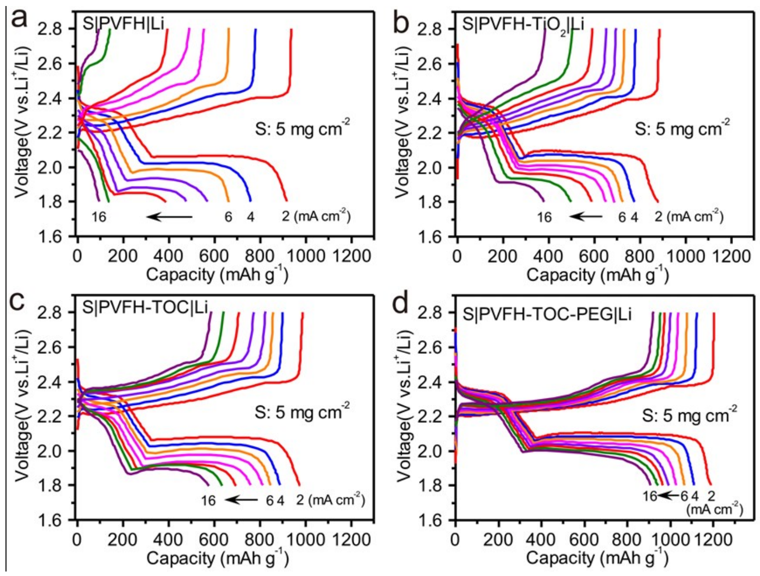

Fig. S19 Representative charge/discharge curves of the (a) S|PVFH|Li, (b) S|PVFH-TiO_2|Li, (c) S|PVFH-TOC|Li, and (d) S|PVFH-TOC-PEG|Li cells from 2 mA cm^{-2} to 16 mA cm^{-2}. As with many of the previously reported GPE Li-S batteries, the plateaus observed in the discharge curves of the S|PVFH-TOC-PEG|Li cell are corresponding to the two redox reactions from S8→ $Li_2S_{4–8}$ → Li_2S_2/Li_2S.

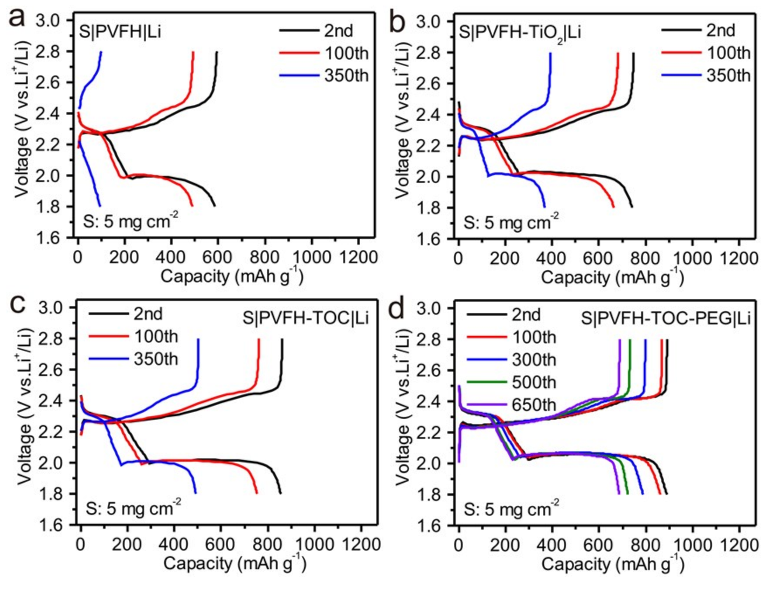

Fig. S20 Charge/discharge curves of the (a) S|PVFH|Li, (b) S|PVFH-TiO_2|Li, (c) S|PVFH-TOC|Li, and (d) S|PVFH-TOC-PEG|Li cells with an E/S ratio of 6 μL mg_S^{-1} at 8 mA cm^{-2}.

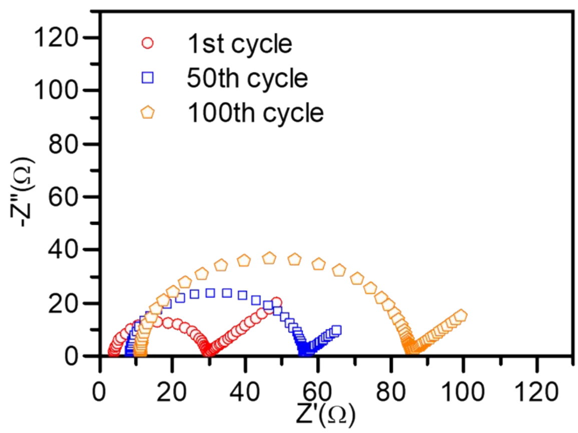

Fig. S21 The EIS tests of the S|PVFH-TOC-PEG|Li cell after different cycles at 8 mA cm^{-2}.

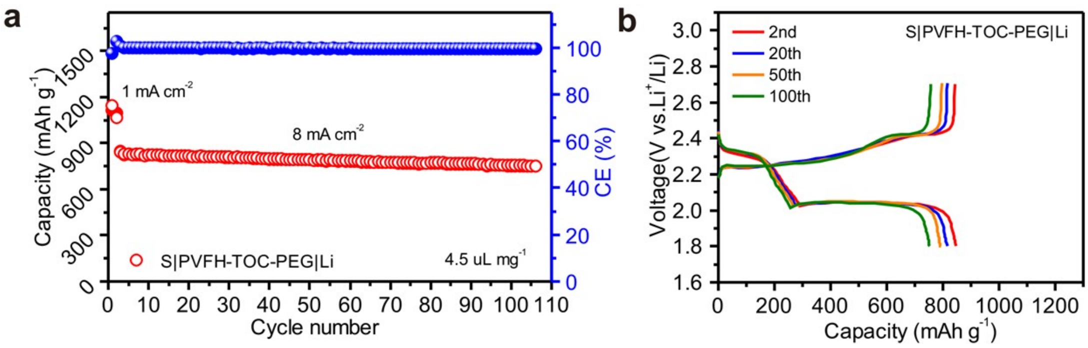

Fig. S22 (a) Cycling performance and (b) charge/discharge curves of the S|PVFH-TOC-PEG|Li cell with a low E/S ratio of 4.5 μL mg_S^{-1}.

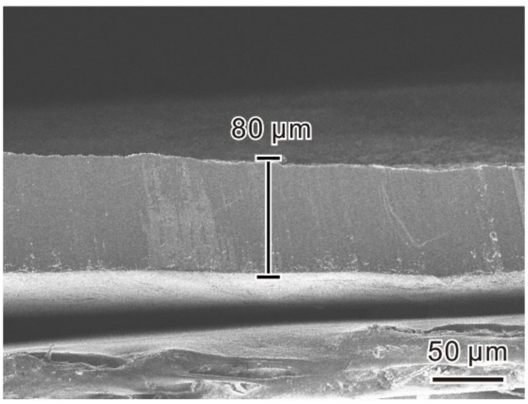

Fig. S23 Cross-section SEM image of the pressed Li foil showing a thickness of 80 μm.

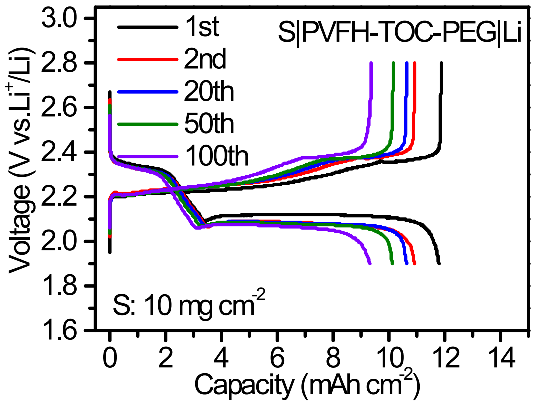

Fig. S24 Charge/discharge curves of the S|PVFH-TOC-PEG|Li cell with an E/S ratio of 3 μL mg_S^{-1} at 2 mA cm^{-2}.

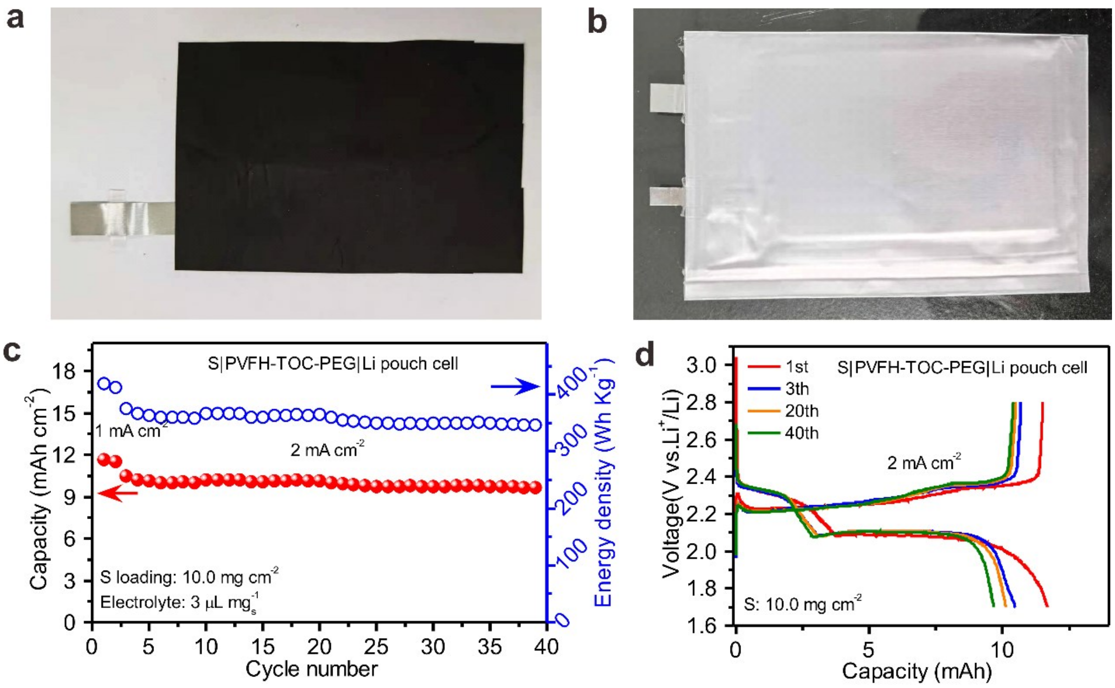

Fig. S25 Optical images of (a) CB/S cathode and (b) S|PVFH-TOC-PEG|Li pouch cell. (c) The energy density and (d) charge/discharge curves of the pouch cell. In this pouch cell, the CB/S cathode with 67 wt% and 10 mg cm^{-2} of sulfur was fabricated on a piece of carbon nanofiber paper. The weights of the CB/S cathode and the carbon nanofiber paper are 14.9 mg cm^{-2} and 1 mg cm^{-2}, respectively. A pressed Li foil (4.29 mg cm^{-2} in weight) was used as the anode. The weight of PVFH-TOC-PEG electrolyte is 40 mg cm^{-2}. The sizes of cathode, Li anode and GPE are 48 mm × 66 mm, 48 mm × 66 mm , and 50 mm × 68 mm, respectively. The gravimetric energy density calculated based on the total weight of carbon nanofiber paper, CB/S cathode, GPE, and Li anode is ~417 Wh kg^{-1}.

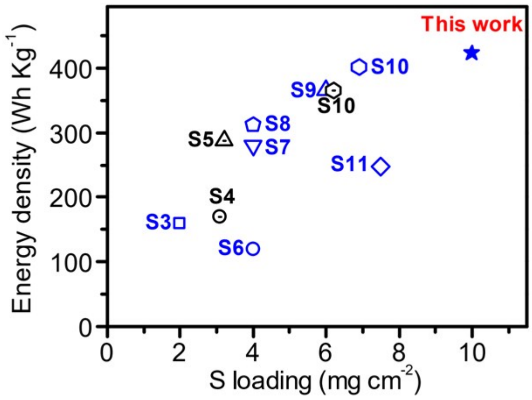

Fig. S26 Comparison of gravimetric energy densities based on this work and the representative Li-S full cells reported recently (See references S3-S11). The blue and black symbols are obtained from coin and punch cells, respectively. The energy densities of coin cells are usually calculated without the package. Since the package mass ratio in pouch cell is about 5 wt%, the energy densities of pouch cells could be multiplied by a factor 1.053 for the qualitative comparison of coin cells and pouch cells.[S7] In addition, the statistical analysis provided by the reference 3 (*Electrochem. Energy Rev.* **1**, 239-293 (2018)) reveals that 95% of the reported Li-S batteries deliver a gravimetric energy density less than 300 Wh kg^{-1}. Obviously, the TOC-reinforced GPE has an advantage in constructing high-energy-density Li-S batteries.

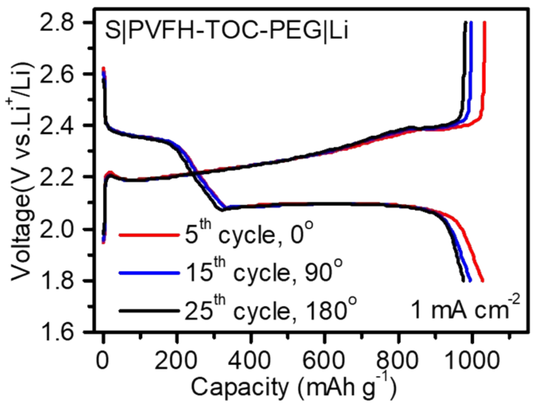

Fig. S27 The charge/discharge curves of the S|PVFH-TOC-PEG|Li battery under the flat, bent, and folded states.

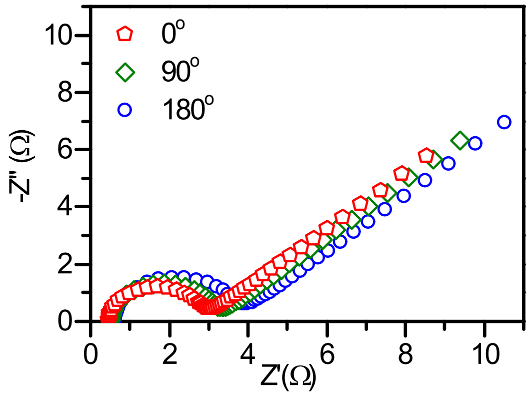

Fig. S28 EIS curves of the S|PVFH-TOC-PEG|Li battery under the flat, bent, and folded states.

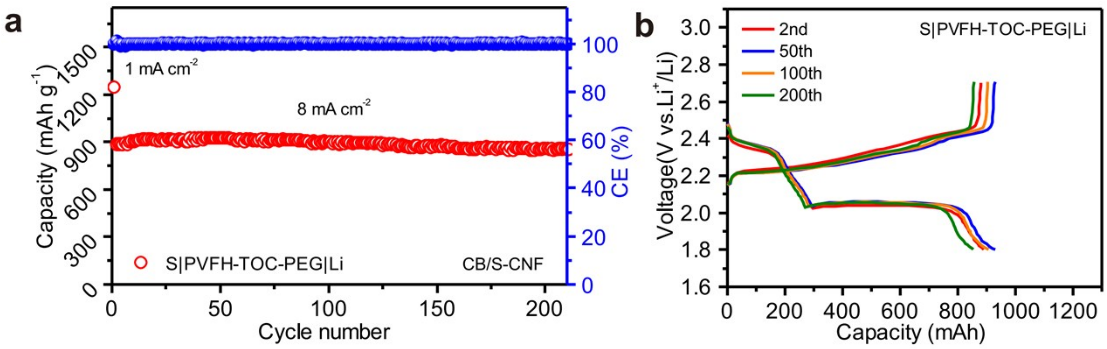

Fig. S29 (a) Cycling performance and (b) charge/discharge curves of the S|PVFH-TOC-PEG|Li coin cell assembled using carbon nanofiber paper. In this coin cell, the sulfur content and areal sulfur loading the CB/S cathode are 67 wt% and 5.0 mg cm^{-2}, respectively, and the E/S ratio is 6 μL mg_S^{-1}.

Table S1. Comparison of the mechanical properties of the PVFH-based membranes.

Sample	Maximum stress (MPa)	Maximum strain (%)
PVFH	26.8	248
PVFH-TiO_2	35.4	345
PVFH-TOC	40.5	455
PVFH-TOC-PEG	**54.2**	**520**

Table S2. The cycling stabilities of the Li|electrolyte|Li symmetric cells.

Electrolyte	Current density and capacity (mA cm^{-2}/mAh cm^{-2})	Cycling time (hrs)	Rate capability (mA cm^{-2})	Ref.
PVFH-TiO_2	0.1/0.1	800	0.1	S1
PEO-SiO_2	0.2/1	500	1	S2
PEGDE-DEBA-DPPO	0.5/0.5	900	2.5	S12
Trimethylolpropane triglycidyl ether	0.5/0.5	560	0.2	S13
PVFH-LLZO-Ga	0.5/ 0.5	1000	0.5	S14
Polymerized $LiPF_6$/DOL	1/1	450	1	S15
PVFH-BN	1/1	1900	1	S16
PVFH-Ionic liquid	1/5	1000	2	S17
TEOS-N,N′-dimethylacrylamide	3/1	300	3	S18
PVFH-TOC-PEG	**1/5**	**2000**	**10**	**This work**

Table S3. Comparison of lean- and flooded-electrolyte Li-S batteries.

S content of cathode (wt%)	S loading (mg cm^{-2})	E/S ratio (μL mg_S^{-1})	Initial capacity (mAh cm^{-2})	Capacity after the cycling test (mAh g^{-1})	Ref.
53	1.5	5	~1.8	~700 (100th cycle at 0.1 C)	S19
64	3-4	5	3.4	~760 (100th cycle at 0.2 C)	S20
52	3.8	4.2	4	~850 (300th cycle at 0.08 C)	S21
64	4	3.3	4.7	~610 (100th cycle at 0.2 C)	S22
75.2	5.1	6	~4.7	765 (300th cycle at 0.2 C)	S23
61	6	4	6.5	~800 (50th cycle at 0.08 C)	S24
65	10	6	~7	~490 (200th cycle at 1 C)	S25
64	4.2	7.5	3.4	~450 (100th cycle at 1 C)	S26
69	5	10	5	700 (100th cycle at 0.2 C)	S27
56	5.2	10	2.3	~420 (350th cycle at 1 C)	S28
56	3.5	10	3.54	820 (150th cycle at 0.2 C)	S29
63	4.8	14	4.2	800 (150th cycle at 0.5 C)	S30
70	2	20	1.5	~447 (600th cycle at 1 C)	S31
64	1	30	0.56	470 (5th cycle at 0.5 C)	S32
61	4.17	30	5.2	~737 (100th cycle at 0.1 C)	S33
52	4.4	68	5.85	682 (200th cycle at 0.15 C)	S34
67	**5**	**6**	**6.3**	**680 (650th cycle at 0.95 C)**	**This work**
	10	**3**	**11.8**	**932 (100th cycle at 0.12 C)**	

References

S1. N. Chen, Y. Xing, L. L Wang, F. Liu, L. Li, R. J. Chen, F. Wu and S. J. Guo, *Nano Energy* 2018, **47**, 35-42.

S2. S. Choudhury, R. Mangal, A. Agrawal and L. A. Archer, *Nat. commun.* 2015, **6**, 10101.

S3. D. C. Lin, J. Zhao, J. Sun, H. B. Yao, Y. Y. Liu, K. Yan and Y. Cui, *PNAS* 2017, **114**, 4613-4618.

S4. J. Y. Hwang, H. M. Kim and Y. K. Sun, *J. Electrochem. Soc.* 2018, *165*, A5006-A5013.

S5. J. Chang, J. Shang, Y. M. Sun, L. K. Ono, D. R. Wang, Z. J. Ma, Q. Y. Huang, D. D. Chen, G. Q. Liu, Y. Cui, Y. B. Qi and Z. J. Zheng, *Nat. Commun.* 2018, **9**, 4480.

S6. F. Pei, A. Fu, W. B. Ye, J. Peng, X. L. Fang, M. S. Wang and N. F. Zheng, *ACS Nano* 2019, **13**, 8337-8346.

S7. X. Li, M. Banis, A. Lushington, X. F. Yang, Q. Sun, Y. Zhao, C. Q. Liu, Q. Z. Li, B. Q. Wang, W. Xiao, C. H. Wang, M. S. Li, J. W. Liang, R. Y. Li, Y. F. Hu, L. Goncharova, H. M. Zhang, T. K. Sham and X. L. Sun, *Nat. commun.* 2018, **9**, 4509.

S8. F. Wu, Y. S. Ye, J. Q. Huang, T. Zhao, J. Qian, Y. Y. Zhao, L. Li, L. Wei, R. Luo, Y. X. Huang, Y. Xing and R. J. Chen, *ACS Nano* 2017, **11**, 4694-4702.

S9. F. Liu, Q. F. Xiao, H. B. Wu, F. Sun, X. Y. Liu, F. Li, Z. Y. Le, L. Shen, G. Wang, M. Cai and Y. F. Lu, *ACS Nano* 2017, **11**, 2697-2705.

S10. W. J. Xue, Z. Shi, L. M. Suo, C. Wang, Z. Q. Wang, H. Z. Wang, K. P. So, A. Maurano, D. W. Yu, Y. M. Chen, L. Qie, Z. Zhu, G. Y. Xu, J. Kong and J. Li, *Nat. Energy* 2019, **4**, 374-382.

S11. K. Fu, Y. H. Gong, G. T. Hitz, D. W. Mcowen, Y. J. Li, S. M. Xu, Y. Wen, L. Zhang, C. W. Wang, G. Pastel, J. Q. Dai, B. Y. Liu, H. Xie, Y. G. Yao, E. D. Wachsman and L. B. Hu, *Energy Environ. Sci.* 2017, **10**, 1568-1575.

S12. Q. W. Lu, Y. B. He, Q. P. Yu, B. H. Li, Y. V. Kaneti, Y. W. Yao, F. Y. Kang and Q. H. Yang, *Adv. Mater.* 2017, **29**, 1604460.

S13. Y. Zhang, Y. Shi, X. C. Hu, W. P. Wang, R. Wen, S. Xin and Y. G. Guo, *Adv. Energy Mater.* 2019, **10**, 1903325.

S14. D. Xu, J. M. Su, J. Jin, C. Sun, Y. D. Ruan, C. H. Chen and Z. Y. Wen, *Adv. Energy Mater.* 2019, **9**, 1900611.

S15. F. Q. Liu, W. P. Wang, Y. X. Yin, S. F. Zhang, J. L. Shi, L. Wang, X. D. Zhang, Y. Zheng, J. J. Zhou, L. Li and Y. G. Guo, *Sci. Adv.* 2018, **4**, eaat5383.

S16. J. Shim, H. J. Kim, B. G. Kim, Y. S. Kim, D. G. Kim and J. C. Lee, *Energy Environ. Sci.* 2017, **10**, 1911-1916.

S17. T. Chen, W. H. Kong, Z. W. Zhang, L. Wang, Y. Hu, G. Y. Zhu, R. P. Chen, L. B. Ma, W. Yan, Y. R. Wang, J. Liu and Z Jin, *Nano Energy* 2018, **54**, 17-25.

S18. L. Yu, S. T. Guo, Y. Lu, Y. Q. Li, X. W. Lan, D. B. Wu, R. G. Li, S. Q. Wu and X. L. Hu, *Adv. Energy Mater.* 2019, **9**, 1900257.

S19. Y. T. Liu, D. D. Han, L. Wang, G. R. Li, S. Liu and X. P. Gao, *Adv. Energy Mater.* 2019, **9**, 1803477.

S20. H. L. Pan, K. S. Han, M. H. Engelhard, R. G. Cao, J. Z. Chen, J. G. Zhang, K. T. Mueller, Y. Y. Shao and J. Liu, *Adv. Funct. Mater.* 2018, **28**, 1707234.

S21. K. Lu, Y. Z. Liu, J. Z. Chen, Z. C. Zhang and Y. W. Cheng, *ACS Nano* 2019, **13**, 14540-14548.

S22. J. Z. Chen, W. A. Henderson, H. L. Pan, B. R. Perdue, R. G. Cao, J. Z. Hu, C. Wan, K. S. Han, K. T. Mueller, J. G. Zhang, Y. Y. Shao and J. Liu, *Nano Lett* 2017, **17**, 3061-3067.

S23. G. Li, W. Lei, D. Luo, Y. P. Deng, Z. P. Deng, D. L. Wang, A. P. Yu and Z. W. Chen, *Energy Environ. Sci.* 2018, **11**, 2372-2381.

S24. Y. X. Yang, Y. R. Zhong, Q. W. Shi, Z. H. Wang, K. N. Sun and H. L. Wang, Angew. Chem. Int. Ed. 2018, **57**, 15549-15552.

S25. S. H. Chung, K. Y. Lai and A. Manthiram, *Adv. Mater.* 2018, **30**, 1805571.

S26. Y. Z. Song, W. Zhao, L. Kong, L. Zhang, X. Y. Zhu, Y. L. Shao, F. Ding, Q. Zhang, J. Y. Sun and Z. F. Liu, *Energy Environ. Sci.* 2018, **11**, 2620-2630.

S27. Y. Z. Wang, D. Adekoya, J. Q. Sun, T. Y. Tang, H. L. Qiu, L. Xu, S. Q. Zhang and Y. L. Hou, *Adv. Funct. Mater.* 2018, **29**, 1807485.

S28. W. Chen, T. Y. Lei, W. Q. Lv, Y. Hu, Y. C. Yan, Y. Jiao, W. D. He, Z. H. Li, C. L. Yan and J. Xiong, *Adv. Mater.* 2018, **30**, 1804084.

S29. T. Chen, Z. W. Zhang, B. R. Cheng, R. P. Chen, Y. Hu, L. B. Ma, G. Y. Zhu, J. Liu and Z. Jin, *J. Am. Chem. Soc.* 2017, **139**, 12710-12715.

S30. M. Zhao, H. J. Peng, Z. W. Zhang, B. Q. Li, X. Chen, J. Xie, X. Chen, J. Y. Wei, Q. Zhang and J. Q. Huang, *Angew. Chem. Int. Ed.* 2019, **58**, 3779-3783.

S31. Y. S. Fu, Z. Wu, Y. F. Yuan, P. Chen, L. Yu, L. Yuan, Q. R. Han, Y. J. Lan, W. X. Bai, E. J. Kan, C. X. Huang, X. P. Ouyang, X. Wang, J. W. Zhu and J Lu, *Nat. commun.* 2020, **11**, 845.

S32. Y. Liu, D. Z. Yang, W. Q. Yan, Q. H. Huang, Y. S. Zhu, L. J. Fu and Y. P. Wu, *iScience* 2019, **19**, 316-325.

S33. Z. S. Wang, J. D. Shen, J. Liu, X. J. Xu, Z. B. Liu, R. Z. Hu, L. C. Yang, Y. Z. Feng, Z. C. Shi, L. Z. Ouyang, Y. Yu and M. Zhu, *Adv. Mater.* 2019, **31**, 1902228.

S34. W. X. Hua, Z. Yang, H. G. Nie, Z. Y. Li, J. Z. Yang, Z. Q. Guo, C. P. Ruan, X. Chen and S. M. Huang, *ACS Nano* 2017, **11**, 2209-2218.